

Photopolymerizable Nanoparticle-polymer Composite Materials for Light and Neutron Beam Manipulations

Yasuo Tomita^{1,†}, Kohta Nagaya¹, Toshi Aoi¹, Yuko Iso¹, Akihisa Kageyama¹, Naoya Nishimura², Keisuke Odoi², Koichi Umemoto³, Jürgen Klepp⁴, Christian Pruner⁵ and Martin Fally⁴

¹*Department of Engineering Science, University of Electro-Communications, Chofu, Tokyo 182-8585, Japan*

²*Materials Research Laboratories, Nissan Chemical Industries, LTD., Funabashi, Chiba 274-0052, Japan*

³*Central Research Center, Daicel Corp., Himeji, Hyogo 671-1283, Japan*

⁴*Faculty of Physics, University of Vienna, Vienna, Austria*

⁵*Department of Materials Science and Physics, University of Salzburg, Salzburg, Austria*

Keywords: Nanocomposite Materials, Photonic Nanostructured Materials, Nanoparticles, Photopolymer, Volume Holographic Grating, Holographic Data Storage, Nonlinear Optics, Neutron Optics.

Abstract: We report on a recent progress in a new class of photopolymerizable nanostructured materials, the so-called photopolymerizable nanoparticle-polymer composites (NPCs). They consist of photoreactive monomer (photopolymer) dispersed with inorganic or organic nanoparticles at high concentrations. The initially uniform distribution of nanoparticles in a neat monomer host is spatially assembled under holographic exposure, providing the single step formation of large scale and multi-dimensional photonic lattice structures in NPC films. This property can be used for versatile applications in photonics and neutron optics such as holographic data storage, holographic optical elements, nonlinear photonic crystals and slow-neutron beam control. Here we describe applications of NPCs dispersed with new organic and inorganic nanoparticles to holographic data storage and holographic diffractive elements for light and neutron beams.

1 INTRODUCTION

Photonic nanostructured materials having spatially ordered arrangements such as photonic crystals and metamaterials have been of considerable interest for their tailored linear and nonlinear optical properties that cannot be usually available by natural materials (Lourtioz et al., 2005; Smith et al., 2004). Another type of nanostructured materials involves either random arrangements of nanoscale materials, *i.e.*, nanoparticles (nanocrystals), embedded in a host material or different materials finely interspersed with/alterd one another. Such nanocomposite materials exhibit the local-field effect that can be also used to control the linear and nonlinear optical properties by various types of spatial arrangements including Maxwell-Garnett, Bruggeman and layered composite geometries (Dolgaleva and Boyd, 2012). However, these nanostructured materials are usually photo-insensitive so that no light control of their arrangement is possible.

As a novel photo-configurable nanostructured material, in 2002 we demonstrated volume holo-

graphic recording in a new type of photopolymerizable organic-inorganic nanocomposite material, the so-called photopolymerizable nanoparticle-polymer composite (NPC) (Tomita et al., 2016a), in which inorganic TiO₂ nanoparticles were highly dispersed in methacrylate photopolymer (Suzuki et al., 2002). The idea of using inorganic nanoparticles possessing a wide variety of refractive indices in the visible is to employ them as transporting species under spatially inhomogeneous illumination (holographic exposure), so that nanoparticles and monomer species mutually diffuse and phase-separate each other to form the spatial density modulation of nanoparticles according to the light-intensity distribution. It would induce large refractive index modulation provided that refractive indices between nanoparticles and the formed polymer are large enough to form higher contrast photonic lattice structures (phase gratings) than those formed in conventional all-organic photopolymer materials under holographic exposure. In addition, the inclusion of inorganic nanoparticles contributes to the improvement of mechanical and thermal stability of the formed photonic lattice structure. Sub-

sequently, we reported volume holographic recording in NPCs using other SiO₂ and ZrO₂ nanoparticles dispersed in (meth)acrylate monomer capable of the chain-growth polymerization. It was shown that the saturated refractive index modulation amplitude (Δn_{sat}) as large as 1×10^{-2} was possible in the blue and the green with reduced polymerization shrinkage and high thermal stability (Suzuki and Tomita, 2004; Suzuki et al., 2006; Tomita et al., 2008; Omura and Tomita, 2010). In order to use inorganic nanoparticle dispersed NPCs for optical recording media in holographic data storage (HDS) (Cofal et al., 2000; Curtis et al., 2010), we proposed NPCs with thiol-ene/thiol-yne monomers capable of the step-growth polymerization (Hata et al., 2011; Mitsube et al., 2014; Kawana et al., 2015). It was shown that a plane-wave holographic grating recorded in such thiol-ene/thiol-yne based NPCs satisfied all the requirements for HDS media, that is, $\Delta n_{\text{sat}} \geq 5 \times 10^{-3}$, the material recording sensitivity higher than 500 cm/J and polymerization shrinkage lower than 0.5 %. We then successfully demonstrated shift-multiplexed holographic digital data page storage in thiol-ene/thiol-yne based NPCs by using a two-beam interference setup (Momose et al., 2012; Mitsube et al., 2014; Takayama et al., 2014).

High dispersion (>20 vol.%) of inorganic nanoparticles in host monomer always requires careful surface treatment for their uniform dispersion without any aggregation. In order to relax this severe requirement, we proposed NPCs dispersed with hyperbranched polymers (HBPs) (Gao and Yan, 2004), nanostructured polymer possessing highly branched main chains, as organic nanoparticles. Indeed, HBPs are preferable because of the ease of their preparation and the controllability of the size and refractive index. Until now we have reported NPCs dispersed with various types of HBPs. These include low refractive index hyperbranched poly(ethyl methacrylate) (HPEMA) and high refractive index hyperbranched polystyrene (HPS) having their refractive indices of 1.51 and 1.61 at a wavelength of 589 nm, respectively (Tomita et al., 2006b). They could be dispersed in multifunctional (meth)acrylate monomer without any aggregation at their concentrations up to 40 vol.%. They gave Δn_{sat} as large as 8×10^{-3} and 7×10^{-3} , respectively, at a recording intensity of 100 mW/cm² and at recording and readout wavelengths of 532 nm. Recently, we also introduced newly developed HBP having the ultrahigh refractive index of 1.82 to increase Δn_{sat} further (Tomita et al., 2016b). An NPC grating incorporated with such an HBP gave Δn_{sat} as large as 2.2×10^{-2} at 532 nm with good optical quality,

suggesting its application to a holographic diffractive element for wearable eyeglasses to be used for augmented and mixed reality by which the real-time and ubiquitous access of virtual 2D/3D images is possible in free space.

One can also utilize the composite nature of NPCs for developing artificial nonlinear optical materials when either guest or both guest and host have distinct optical nonlinearities. So far, optical nonlinearities of metal-dielectric nanocomposites were reported by many workers (Hache et al., 1988), where the surface plasmon resonance (SPR) (Klar et al., 1998) taking place at the interface between metallic nanoparticles and a dielectric host was used to induce the optical nonlinearity due to the coherent oscillation of free electrons occupying states near the Fermi level in the conduction band. This SPR resulted in the local-field enhancement (Dolgaleva and Boyd, 2012), leading to the enhancement of the optical nonlinearities of metal-dielectric nanocomposites. We studied the nonlinear optical properties of holographically recordable NPCs dispersed with HBP-metallic (Au or Pt) nanoparticle complex (Liu et al., 2010). It was shown that they exhibited the dielectric confinement effect near SPR and that the magnitude of their effective third-order nonlinear optical susceptibility was of the order of 10^{-10} esu at a wavelength of 532 nm. We also investigated the optical nonlinearity in a semiconductor CdSe quantum dot dispersed NPC film (Liu et al., 2012). Because of the composite structure cascaded high order optical nonlinearities were observed. Associated nonlinear Bragg diffraction from the 1D photonic lattice structure recorded in the NPC film were also observed.

Volume gratings recorded in NPCs can find completely different applications from those in optics and photonics. Namely, matter waves can be manipulated by diffraction from gratings, where such an incoming beam interacts with periodically assembled nuclei via the strong (nuclear) force. Neutrons have been extensively used for scientific and engineering studies. In particular, neutron optics and spectroscopy have been deployed for nuclear physics, quantum physics, condensed matter physics, biology, life and medical sciences, materials science and engineering (Sears, 1989; Rauch and Werner, 2015; Klepp et al., 2014; Willis and Carlile, 2013). For some of these purposes efficient neutron optical elements such as mirrors and beam splitters are essential, for example, to construct a neutron interferometer. A perfect silicon crystal is employed to diffract a thermal neutron beam at neutron wavelengths λ_{neu} shorter than 0.4 nm. Because the phase in neutron interferometer is proportional to λ_{neu} (Rauch and Werner, 2015), as opposed to the in-

verse wavelength law in optics, slow neutrons (cold and very cold neutrons) at longer wavelengths ($0.4 \text{ nm} < \lambda_{\text{neu}} < 10 \text{ nm}$) are advantageous. However, slow-neutron optics requires other neutron optical elements as Bragg's law cannot be satisfied for slow neutron beams with perfect silicon crystals. For this reason Rupp *et al.* demonstrated the diffraction of a cold neutron beam ($\lambda_{\text{neu}} = 1.5 \text{ nm}$) by a holographic volume grating optically recorded in PMMA-based photopolymer with deuterium substitution (Rupp *et al.*, 1990). Despite their successful proof-of-principle demonstration the diffraction efficiency was severely limited by the Pendellösung oscillation (Klepp *et al.*, 2012a) that averaged out the diffraction efficiency due to the very thick film ($\sim 2 \text{ mm}$) and the limited collimation of an incident slow neutron beam. By taking advantage of the composite nature of NPCs, we developed neutron optical elements by use of a volume grating optically recorded in a $100\text{-}\mu\text{m}$ thick NPC film dispersed with SiO_2 nanoparticles that have substantive interaction strength with slow neutrons. We successfully demonstrated manipulation of slow neutron beams such as beam splitting, triple beam division and mirror operations (Fally *et al.*, 2010; Klepp *et al.*, 2011; Klepp *et al.*, 2012b; Klepp *et al.*, 2012c).

In this paper we first describe the grating formation mechanism in NPCs and discuss material's design parameters governing Δn_{sat} . Then we describe applications of NPCs dispersed with new organic and inorganic nanoparticles to holographic data storage and holographic diffractive elements for light and neutron beams.

2 GRATING FORMATION MECHANISM

Here we describe the grating formation in an NPC film where nanoparticles are uniformly dispersed in host monomer capable of radical photopolymerization, as shown in Fig.1(a). Photoinitiator species locally generate free radicals by their dissociation under two-beam interfering exposure and the subsequent reaction of free radicals with monomer leads to the polymerization reaction between monomer radicals and unreacted monomer in the bright regions. This polymerization process lowers the chemical potential of unreacted monomer in the bright regions, leading to the diffusion of unreacted monomer from the dark to the bright illuminated regions. Because nanoparticles are photo-insensitive and their chemical potential increases as a result of the monomer consumption in the bright illuminated regions, nanoparticles counter-diffuse from the bright to the dark illuminated

regions. In this way the mutual diffusion and the phase separation of monomer and nanoparticles lead to the spatial density modulation of nanoparticles during holographic exposure [see Fig.1(b)]. Such holographic assembly of nanoparticles in the formed polymer host (Tomita *et al.*, 2005) results in the formation of a refractive index grating due to the density and compositional differences between the bright and the dark illuminated regions. This model was confirmed experimentally as shown in Figs. 1(c) and 1(d) that show electron-probe micro-analyzer (EPMA) images of density distributions of Si and S atoms, respectively (Tomita *et al.*, 2006a), where Si and S atoms correspond to constituents of nanoparticles and the formed polymer.

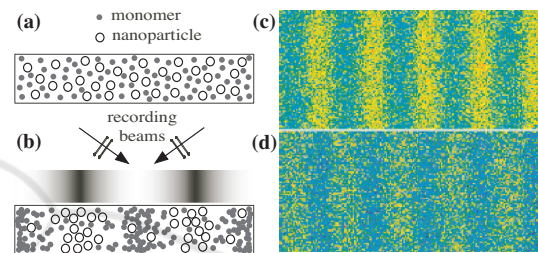


Figure 1: Holographic assembly of nanoparticles in an NPC material (a) before and (b) after holographic exposure. EPMA images of (c) Si (nanoparticles) and (d) S (the formed polymer) atomic density distributions after holographic exposure.

It can be shown that Δn_{sat} for the 1st-order periodic spatial modulation of the refractive index in an NPC as a multi-component photopolymer system is approximately given by (Tomita *et al.*, 2016a)

$$\Delta n_{\text{sat}} = a\Delta f(n_n - n_p), \quad (1)$$

where a is a form factor depending on a waveform of the density modulation of nanoparticles and Δf is a difference in the volume fraction of dispersed nanoparticles between the peak and the average volume fraction f of the nanoparticles. Also, n_n (n_p) is the refractive index of the nanoparticle (the formed host polymer), respectively. The value for a is unity for a sinusoidal waveform and is $2 \sin(r\pi)/\pi$ for a rectangular waveform with the duty ratio r . It can be seen that Δf and $|n_n - n_p|$ are major material's design parameters that determine Δn_{sat} . It is easy to find that Δf takes values between 0 and f at $0 \leq f \leq 0.5$ and between 0 and $1 - f$ at $0.5 \leq f \leq 1$. Thus, Δf is maximized to be 0.5 at $f = 0.5$ and the density modulation index of nanoparticles defined as $\Delta f/f$ is unity. In practice, however, an increase in f larger than, say, 0.4 causes substantive holographic light scattering (Suzuki and Tomita, 2007) during recording when $|n_n - n_p|$ is very large for a very thick NPC

film dispersed with nanoparticles having ~ 10 nm in size. This situation would reduce Δn_{sat} . For this reason $\Delta f = f \sim 0.4$ would be a practical maximum limit.

3 HOLOGRAPHIC DATA STORAGE

As described in the introduction part, we developed thiol-ene/thiol-yne based NPCs for HDS media and employed them in shift-multiplexed holographic digital data page storage by using a two-beam interference method (Momose et al., 2012; Mitsube et al., 2014; Takayama et al., 2014). Here we describe their use in coaxial holographic recording setup (Horimai et al., 2005). Figure 2 illustrates our optical setup for a holographic digital data page recording using the coaxial holographic recording setup. The linearly polarized laser beam at a recording and readout wavelength of 532 nm was expanded and collimated to encode a circular and concentric input page pattern for digital signal and reference data with the 9:16 symbol modulation coding format (Takayama et al., 2014) [see Fig. 3(a)] via a transmission-type liquid crystal spatial light modulator (HOLOEYE Photonics LC2002) with 1024 \times 768 pixels and a pixel pitch of 36 μm . The size of one data page [the circular portion in Fig. 3(a)] had 12969 bits that corresponded to 14441 symbol data of information. No error correction coding (ECC) was made. The transmitted data-bearing beam was loosely focused on an NPC film sample of 100- μm thickness via two relay lenses and an objective lens. For thiol-ene based NPC film samples we employed the stoichiometric thiol-ene formulation of commercial secondary dithiol monomer, 1,4-bis(3-mercaptopbutyryloxy)butane (Showa Denko K.K.), and triene monomer, 1, 3, 5-triallyl-triazine-2,4,6(1H,3H,5H)-trione (Sigma-Aldrich), to-

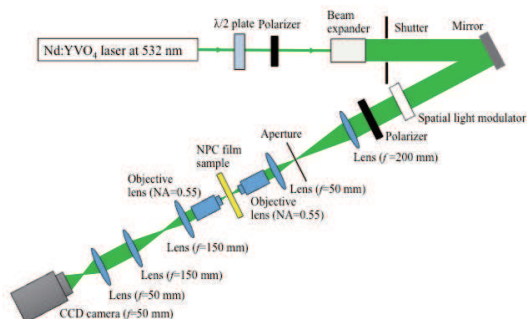


Figure 2: Setup for coaxial holographic digital data page recording.

gether with the dispersion of 25 vol.% SiO_2 nanoparticles (the average size of 13 nm) and a photoinitiator/green-sensitizer system consisting of Irgacure 784 (Ciba) and BzO_2 (Sigma-Aldrich) at 1 and 1.25 wt.%, respectively, with respect to the thiol-ene monomer blend. For thiol-yne based NPC film samples we employed the stoichiometric thiol-yne monomer blend consisting of commercial trithiol monomer, trimethylolpropane tris(3-mercaptopropionate) (Sigma-Aldrich), and diene monomer, 1, 7-octadiyne (Sigma-Aldrich). It was mixed with a co-monomer at 15 wt.% with respect to the thiol-yne monomer blend, N-vinyl-2-pyrrolidone (Sigma-Aldrich), acting as a plasticizer for the uniform dispersion of 25 vol.% SiO_2 nanoparticles. A photoinitiator/green-sensitizer system consisting of Irgacure 784 and BzO_2 at 1 and 1.25 wt.%, respectively, with respect to the thiol-yne monomer blend were also mixed. The reconstructed straight-through image through a uniformly cured thiol-ene NPC film sample by an incoherent LED is shown in Fig. 3(b). The symbol error rate (SER) and the signal-to-noise ratio (SNR) are found to be 7.7×10^{-5} and 14, respectively. The reconstructed image from a recorded thiol-ene based NPC film sample is shown in Fig. 3(c) by which SER and SNR are found to be 7.7×10^{-5} and 12, respectively. Figure 3(d) shows the reconstructed

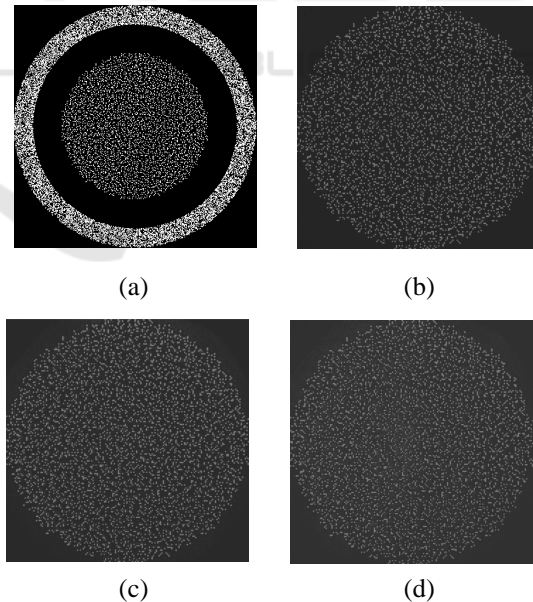


Figure 3: (a) Digital data page pattern with the 9:16 symbol modulation code. (b) Magnified image of the straight-through image via a uniformly cured thiol-ene based NPC film. (c) Magnified image of the reconstructed digital data page pattern from a recorded thiol-ene based NPC film. (d) Magnified image of the reconstructed digital data page pattern from a recorded thiol-yne based NPC film.

image from a recorded thiol-yne NPC film sample, giving SER and SNR of 7.7×10^{-5} and 11, respectively. It is known that error-free retrieval of data pages with an SER of lower than 1×10^{-1} is possible with ECC (Tanaka et al., 2007). Therefore, the measured performance suggests that error-free retrieval of digital data pages is possible with our thiol-ene/thiol-yne based NPCs.

4 HOLOGRAPHIC DIFFRACTIVE ELEMENTS

4.1 Light Beams

Holographic diffractive elements usually require high diffraction efficiencies near 100%. This is possible when a volume phase grating is thick enough to meet the conditions that the product of the coupling constant $\kappa (\equiv \pi \Delta n_{\text{sat}} / \lambda \cos \theta_B)$ and the grating thickness L be near $(2m - 1)\pi/2$ ($m = 1, 2, \dots$) for a transmission grating and be larger than, say, 2 for a reflection grating in light optics (Yeh, 1993). Here λ is a readout wavelength in vacuum and θ_B is the Bragg angle in the volume grating. The latter is measured from the optical axis for an incident readout beam. There is often another requirement for wide angular and/or wavelength selectivities (*i.e.*, the angular aperture and/or spectral bandwidth of the Bragg diffraction) for specific applications. In this case the selectivity of a volume grating is inversely proportional to L . For narrowband optical filters, holographic sensors, and holographic data storage a thick volume grating of the order of $100 \mu\text{m}$ is preferable. On the other hand, a thin volume grating near $10 \mu\text{m}$ is desired for applications such as wearable eyeglasses used for augmented and mixed reality, which requires high diffraction efficiencies at wide acceptable angles (*i.e.*, with a wide Bragg aperture). In such a case the diffraction efficiency near 100% requires Δn_{sat} to be larger than $\sim 2.5 \times 10^{-2}$ for transmission and reflection volume gratings of $10 \mu\text{m}$ thickness at a visible wavelength. NPCs would be suitable for such an application because of the ease of their coating on curved eyeglass surfaces and the potentiality of increasing Δn_{sat} by a suitable choice of nanoparticles according to the material's design strategy based on Eq. (1).

Here we show our recent result of transmission NPC volume gratings dispersed with HBP organic nanoparticles with the ultrahigh refractive index. We synthesized HBP containing triazine and aromatic ring units [see Fig. 4(a)] and the average

size was approximately 12 nm estimated by a small angle X-ray scattering method. The refractive index was found to be 1.82 at a wavelength of 532 nm, which was much higher than those of HPEMA and HPS used for NPCs in our past work (Tomita et al., 2006b). Such an ultrahigh value can be attributed to the incorporation of triazine and aromatic ring units to the HBP structure. We mixed this HBP with single functional monomers, tetrahydrofurfuryl acrylate (THF-A, TCI) and N-vinyl-2-pyrrolidone (NVP, Sigma-Aldrich), used as plasticizers. In this work we employed multifunctional acrylate monomer ($n_D=1.48$), di-pentaerythritol polyacrylate (A-DPH-12E, Shin-Nakamura Chem. Co. Ltd) [see Fig. 4(b)], to the mixture to form the high cross-linked structure after curing and increase the recording sensitivity as compared to that of more viscous multifunctional monomer, dipentaerythritol penta-/hexa-acrylate (DPHA, TOAGOSEI Co., Ltd.), used in our previous work (Tomita et al., 2016b). The resultant concentration ratio of THF-A: NVP: A-DPH-12E in vol.% was 63:5:5 when the HBP concentration was fixed to be 27 vol.%, the maximum doping concentration of HBP. A green photosensitizer Irgacure 784 (Ciba) was also added to the monomer blend of THF-A, NVP, and A-DPH-12E, at 1.5 wt.% with respect to A-DPH. The mixed syrup was cast on a glass plate loaded with a $10\text{-}\mu\text{m}$ thick spacer and was finally covered with another glass plate for holographic recording.

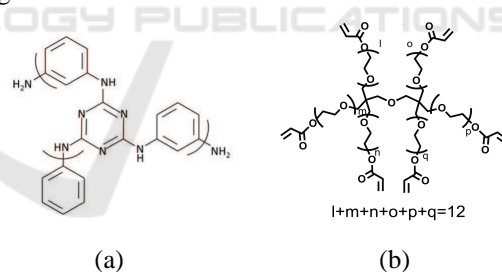


Figure 4: Chemical structures of (a) HBP and (b) A-DPH-12E.

We used a two-beam interference setup to write an unslanted and plane-wave transmission volume grating at $1\text{-}\mu\text{m}$ grating spacing by two mutually coherent beams of equal intensities at a wavelength of 532 nm. A low-intensity He-Ne laser beam operating at a photoinitiator-insensitive wavelength of 633 nm was employed as a readout beam to monitor the buildup dynamics of the grating. All the beams were s-polarized. Figure 5 shows photographs of a volume grating recorded in an NPC sample. Good uniformity and high transparency of the volume grating are seen. Figure 6(a) shows the recording dynamics of the diffraction efficiency, defined as the ratio

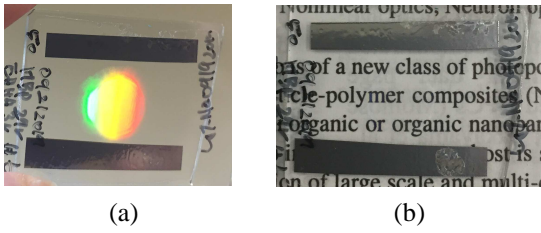


Figure 5: (a) Photograph of an NPC volume grating under white light illumination from a fluorescent lamp. (b) Photograph of the same grating viewed from the top.

of the 1st-order diffracted signal power to the sum of the transmitted and the 1st-order diffracted beam powers, at a readout wavelength of 633 nm and at a recording intensity of 75 mW/cm^2 . The inset is a Bragg-angle detuning dependence of the saturated diffraction efficiency probed at 633 nm. The solid curve denotes the least-squares curve fit of the data to Kogelnik's formula (Kogelnik, 1969). A good fit of the data to the formula with the correlation coefficient higher than 0.99 indicates the uniformity of the recorded NPC volume grating along the thickness di-

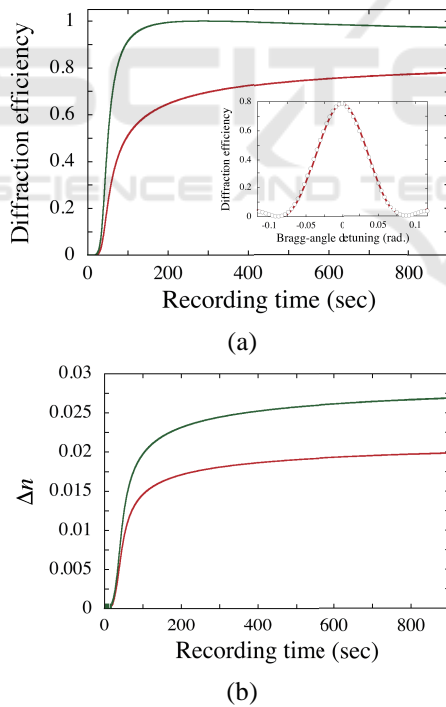


Figure 6: (a) Recording dynamics of the diffraction efficiency probed by a 633-nm laser beam at a recording intensity of 75 mW/cm^2 . The curve in green is the extrapolated recording dynamics of the diffraction efficiency at 532 nm as described in the text. The inset is a Bragg-angle detuning dependence of the diffraction efficiency probed at 633 nm. (b) Buildup dynamics of Δn at wavelengths of 532 nm (green) and 633 nm (red).

rection. It was determined that the effective thickness ℓ_{eff} of the recorded NPC volume grating was $10.8 \mu\text{m}$. The extrapolated recording dynamics of the diffraction efficiency at 532 nm (the curve in green) was also plotted in Fig. 6(a) by measuring the saturated diffraction efficiency at 532 nm together with Δn_{sat} at 532 nm and ℓ_{eff} as described below. It can be seen that the diffraction efficiency at 532 nm finally saturates below 100% due to the overmodulation effect. Figure 6(b) shows the corresponding buildup dynamics of the refractive index modulation amplitude Δn that was extracted from measured diffraction efficiency data by ℓ_{eff} and Kogelnik's formula. In this extraction procedure estimated values for Δn at 633 nm were converted to those at 532 nm by multiplying the former by a factor being the ratio of Δn_{sat} measured at 532 nm to that measured at 633 nm. We found that Δn_{sat} at 532 nm was 2.7×10^{-2} , larger than 2.2×10^{-2} obtained by our previous NPC composition with DPHA (Tomita et al., 2016b). Furthermore, the recording intensity (75 mW/cm^2) was lower than a half of that with the previous one (200 mW/cm^2) due to the use of A-DPH having higher photochemical reactivity and lower viscosity than those of DPHA. Using Eq. (1), we could estimate Δf to be 0.09 at $a=1$ (the sinusoidal modulation) and 0.14 at $a = \pi/2$ (the rectangular modulation at $r = 0.5$). Therefore, further increase in Δn_{sat} would be possible.

4.2 Neutron Beams

Until now we have successfully demonstrated various manipulation schemes for slow-neutron beams (*e.g.*, beam splitting, triple beam division and total beam deflection) via transmission volume gratings recorded in NPCs dispersed with SiO_2 and ZrO_2 nanoparticles (Fally et al., 2010; Klepp et al., 2012b; Klepp et al., 2012c). As shown in Fig. 7, however, it was necessary to effectively increase the interaction length of an NPC transmission grating by tilting it at a large angle ζ ($\sim 70^\circ$) so that the diffraction efficiency can approach near 100% due to the Pendellösung interference effect [see, for example, (Sears, 1989) and for the particular method see (Somenkov et al., 1978)]. Note that the tilt at $\sim 70^\circ$ corresponds to an effective increase in L by a factor of $1/\cos 70^\circ \sim 2.9$. Such a large increase in thickness by the grating tilt is detrimental in device applications owing to a substantive increase in incoherent scattering and absorption loss for a slow-neutron beam propagating in supporting glass substrates and an NPC material.

In order to avoid such a grating tilt, we need to increase Δn_{sat} for neutrons. In neutron optics n_n and n_p in Eq. (1) must be given at slow-neutron wave-

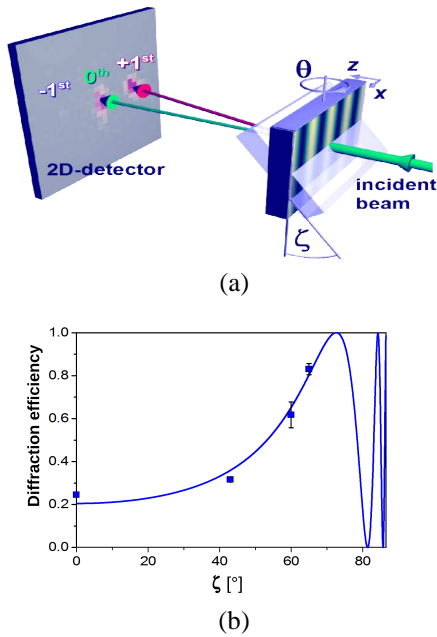


Figure 7: (a) Recording dynamics of the diffraction efficiency probed by a 633-nm laser beam at a recording intensity of 75 mW/cm^2 . (a) Schematic of the slow-neutron beam diffraction via an NPC transmission grating. (b) Peak (Bragg-matched) diffraction efficiencies η_p as a function of NPC grating's tilt angle ζ for an incident very cold neutron beam at a neutron wavelength of 3.76 nm, while the solid curve is a theoretical plot (Klepp et al., 2011).

lengths. The neutron refractive index n_{neu} of a non-magnetic material is approximately given by (Klepp et al., 2012a)

$$n_{\text{neu}} = 1 - \frac{\lambda_{\text{neu}}^2 b_c \rho}{2\pi}, \quad (2)$$

where b_c is the average mean coherent scattering length for a particular isotope and ρ is the atomic number density of the material. Therefore, the factor $n_n - n_p$ in Eq. (1) is determined by a difference in $b_c \rho$ between dispersed nanoparticles and host monomer. For the core SiO_2 material of nanoparticles used in our measurement [see Fig. 7(b)] $b_c \rho$ is given by $3.64 \times 10^{-6}/\text{\AA}^2$. It is well known that diamond possesses very high coherent and very low incoherent scattering cross sections with low absorption for neutrons as compared with other materials. Diamond has $b_c \rho$ of $1.17 \times 10^{-5}/\text{\AA}^2$, which is approximately three times larger than that of SiO_2 . It implies that Δn_{sat} of NPC gratings dispersed with nanodiamonds is three times larger than that of NPC gratings dispersed with SiO_2 nanoparticles. It follows immediately that no grating tilt is necessary to obtain high diffraction efficiency.

Recently, we have investigated the possibility of using nanodiamond for NPC volume gratings. Here

we describe our proof-of-principle result below. Nanodiamonds were prepared by the explosion method and then were made some surface treatment on the core of a nanodiamond (4 nm in diameter) for good dispersion in host monomer. We could successfully disperse nanodiamonds at the concentration of 19 vol.% in an acrylate monomer blend. A green photosensitizer Irgacure 784 (Ciba) was also added at the concentration of 4.3 wt.%. Figure 8(a) illustrates a photograph of an NPC transmission plane-wave grating at grating spacing of $1 \mu\text{m}$ recorded by two 532-nm lasers at the total intensity of 100 mW/cm^2 . The definite diffraction from an area ($\sim 1 \text{ cm}$ in diameter) can be seen. Figure 8(b) shows a transmission-electron microscope image of the cross section of the grating. The dark (bright) banded areas correspond to high concentration portions of nanodiamonds (the formed polymer), showing holographic assembly of nanodiamonds in the formed polymer.

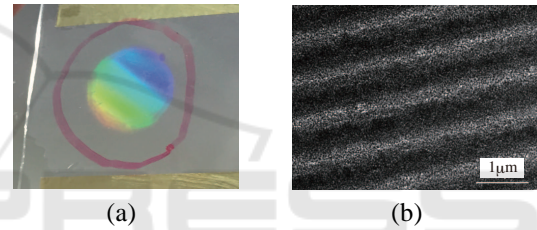


Figure 8: (a) A photograph of an NPC transmission plane-wave grating at grating spacing of $1 \mu\text{m}$ under white light illumination from a fluorescent lamp. (b) A transmission-electron microscope image of the cross section of the grating.

Figure 9(a) shows the Bragg-angle detuning curve probed at 633 nm for the saturated NPC grating. The solid curve denotes the least-squares curve fit of the data to Kogelnik's formula, giving ℓ_{eff} to be $33 \mu\text{m}$. Figure 9(b) shows the buildup dynamics of Δn at 532 nm, which was extracted as similar to the way described above. We found that Δn_{sat} was 2.7×10^{-3} . We estimated the density modulation of nanodiamonds by using the measured value for Δn_{sat} and the refractive indices of nanodiamonds and the formed monomer blends. We found Δf to be 0.006 at $a = 1$ and 0.010 at $a = \pi/2$ and $r = 0.5$, approximately one order smaller than that of the HBP dispersed NPC grating shown in Fig. 6. This result suggests that the mutual diffusion of nanodiamonds and monomer needs to be facilitated much more for an increase of Δf . Our investigation is underway to increase Δf in nanodiamond-dispersed NPC gratings and apply them to neutron diffraction experiments. It would also be expected that nanodiamonds dispersed NPC gratings are useful for holographic applications

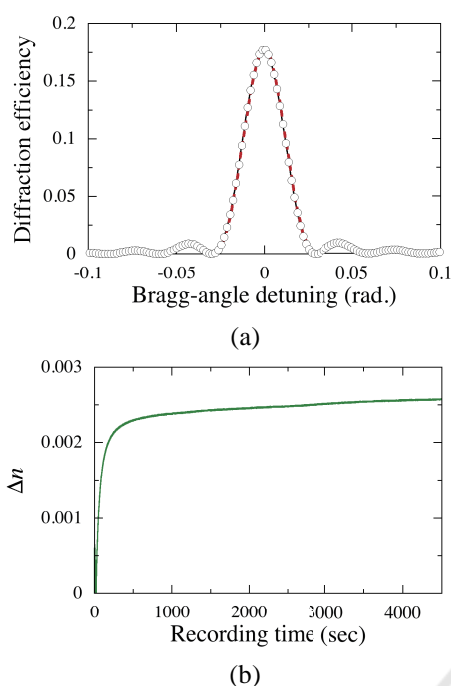


Figure 9: (a) Bragg-angle detuning dependence of the diffraction efficiency at 633 nm. (b) Buildup dynamics of Δn at wavelengths of 532 nm.

in light optics because of very high refractive index ($n_D=2.417$) of bulk diamond in the visible spectral region.

Finally, it should be noted that we have recently succeeded volume holographic recording in NPCs dispersed with superparamagnetic Fe_3O_4 nanoparticles. Such magnetic nanoparticle dispersed NPC gratings have potential applications such as slow-neutron beam's spin control (Klepp et al., 2012a; Tomita et al., 2016a; Ličen et al., 2017) as well as magneto-optic devices in light optics (Tomita et al., 2005).

5 CONCLUSIONS

We have described the mechanism of the holographic grating formation in NPCs and our recent results for holographic applications to holographic data storage and to holographic diffractive elements in light and neutron optics. It has been shown that thiol-ene/thiol-yne based NPCs provide excellent performance with satisfactorily low SERs and high SNRs in a coaxial holographic digital data page recording system. It has also been shown that transmission gratings recorded in NPCs dispersed ultrahigh refractive index HBP give Δn_{sat} close to 3×10^{-2} at moderate grating spacing, promising for holographic diffractive elements in light optics. In addition, we have successfully demon-

strated volume holographic recording in NPCs dispersed with nanodiamonds that possess very high coherent and very low incoherent scattering cross sections with low absorption for neutrons. It can be expected that nanodiamonds dispersed NPC grating provide a new possibility of slow-neutron beam control.

ACKNOWLEDGEMENTS

The authors would like to thank a number of collaborators, including E. Hata, K. Mitsube, K. Momose, S. Takayama, K. Chikama, P. Geltenbort (ILL, Grenoble, France), and J. Kohlbrecher (PSI, Villigen, Switzerland) for their contribution to this work. This work was supported by the Ministry of Education, Culture, Sports, Science and Technology of Japan under the grant numbers 15H03576 and 17K19072.

REFERENCES

- Coufal, H. J., Psaltis, D., and Sincerbox, G. T., editors (2000). *Holographic Data Storage*. Springer, Berlin.
- Curtis, K., Dhar, L., Hill, A. J., Wilson, W. L., and Ayres, M. R., editors (2010). *Holographic Data Storage From Theory to Practical Systems*. Wiley, West Sussex.
- Dolgaleva, K. and Boyd, R. W. (2012). Local-field effects in nanostructured photonic materials. *Advances in Optics and Photonics*, 4:1–77.
- Fally, M., Klepp, J., Tomita, Y., Nakamura, T., Pruner, C., Ellabban, M. A., Rupp, R. A., Bichler, M., Drevnšek-Olenik, I., Kohlbrecher, J., Eckerlebe, H., Lemmel, H., and Rauch, H. (2010). Neutron optical beam splitter from holographically structured nanoparticle-polymer composites. *Physical Review Letters*, 105:123904–1–123904–4.
- Gao, C. and Yan, D. (2004). Hyperbranched polymers: from synthesis to applications. *Progress in Polymer Science*, 29:183–275.
- Hache, F., Ricard, D., Flytzanis, C., and Kreibig, U. (1988). The optical kerr effect in small metal particles and metal colloids: The case of gold. *Applied Physics A*, 47:347–357.
- Hata, E., Mitsube, K., Momose, K., and Tomita, Y. (2011). Holographic nanoparticle-polymer composites based on step-growth thiol-ene photopolymerization. *Optical Materials Express*, 1:207–222.
- Horimai, H., Tan, X., and Li, J. (2005). Collinear holography. *Applied Optics*, 24:16196–16209.
- Kawana, M., Takahashi, J., Yasui, S., and Tomita, Y. (2015). Characterization of volume holographic recording in photopolymerizable nanoparticle-(thiol-ene) polymer composites at 404 nm. *Journal of Applied Physics*, 117:053105–1–053105–6.

- Klar, T., Perner, M., Grosse, S., von Plessen, G., Spirkl, W., and Feldmann, J. (1998). Surface-plasmon resonances in single metallic nanoparticles. *Physical Review Letters*, 80:4249–4252.
- Klepp, J., Pruner, C., Tomita, Y., Geltenbort, P., Drevenšek-Olenik, I., Gyergyek, S., Kohlbrecher, J., and Fally, M. (2012a). Holographic gratings for slow-neutron optics. *Materials*, 2012:2788–2815.
- Klepp, J., Pruner, C., Tomita, Y., Mitsube, K., Geltenbort, P., and Fally, M. (2012b). Mirrors for slow neutrons from holographic nanoparticle-polymer free-standing film-gratings. *Applied Physics Letters*, 100:214104–1–214104–3.
- Klepp, J., Pruner, C., Tomita, Y., Plonka-Spehr, C., Ivanov, S., Geltenbort, P., Kohlbrecher, J., Ellabban, M. A., and Fally, M. (2011). Neutron diffraction by holographic gratings recorded in SiO₂ nanoparticle-polymer composites. *Physical Review A*, 84:013621–1–013621–7.
- Klepp, J., Sponar, S., and Hasegawa, Y. (2014). Fundamental phenomena of quantum mechanics explored with neutron interferometers. *Progress of Theoretical and Experimental Physics*, 2014:082A01–1–082A01–61.
- Klepp, J., Tomita, Y., Pruner, C., Kohlbrecher, J., and Fally, M. (2012c). Three-port beam splitter for cold neutrons using holographic nanoparticle-polymer composite diffraction gratings. *Applied Physics Letters*, 101:154104–1–154104–3.
- Kogelnik, H. (1969). Coupled wave theory for thick hologram gratings. *The Bell System Technical Journal*, 48:2909–2947.
- Liu, X., Adachi, Y., Tomita, Y., Oshima, J., Nakashima, T., and Kawai, T. (2012). High-order nonlinear optical response of a polymer nanocomposite film incorporating semiconductor CdSe quantum dots. *Optics Express*, 20:13457–13469.
- Liu, X., Matsumura, K., Tomita, Y., Yasui, K., Kojima, K., and Chikama, K. (2010). Nonlinear optical responses of nanoparticle-polymer composites incorporating organic (hyperbranched polymer)-metallic nanoparticle complex. *Journal of Applied Physics*, 108:073102–1–073102–9.
- Ličen, M., D.-Olenik, I., Čoga, L., Gyergyek, S., Kralj, S., Fally, M., C.Pruner, P.Geltenbort, Gasser, U., Nagy, G., and Klepp, J. (2017). Neutron diffraction from superparamagnetic colloidal crystals. *Journal of Physics and Chemistry of Solids*, 110:234–240.
- Lourtioz, J.-M., Benisty, H., Berger, V., Gérard, J.-M., and Mystre, D. (2005). *Photonic Crystals*. Springer, Berlin.
- Mitsube, K., Nishimura, Y., Nagaya, K., Takayama, S., and Tomita, Y. (2014). Holographic nanoparticle-polymer composites based on radical-mediated thiol-yne photopolymerizations: Characterization and shift-multiplexed holographic digital data page storage. *Optical Materials Express*, 4:982–996.
- Momose, K., Takayama, S., Hata, E., and Tomita, Y. (2012). Shift-multiplexed holographic digital data page storage in a nanoparticle-(thiol-ene) polymer composite film. *Optics Letters*, 37:2250–2252.
- Omura, K. and Tomita, Y. (2010). Photopolymerization kinetics and volume holographic recording in ZrO₂ nanoparticle-polymer composites at 404 nm. *Journal of Applied Physics*, 107:023107–1–023107–6.
- Rauch, H. and Werner, S. A. (2015). *Neutron Interferometry*. Oxford University Press, Oxford, 2nd edition.
- Rupp, R. A., Hehmann, J., Matull, R., and Ibel, K. (1990). Neutron diffraction from photoinduced gratings in a PMMA matrix. *Physical Review Letters*, 64:301–302.
- Sears, V. F. (1989). *Neutron Optics*. Oxford University Press, Oxford.
- Smith, D. R., Pendry, J. B., and Wiltshire, M. C. K. (2004). Metamaterials and negative refractive index. *Science*, 305:788–792.
- Somenkov, V. A., Shilstein, S. S., Belova, N. E., and Utemisov, K. (1978). Observation of dynamical oscillations for neutron scattering by Ge crystals using the inclination method. *Solid State Communications*, 25:593–595.
- Suzuki, N. and Tomita, Y. (2004). Silica nanoparticles-dispersed methacrylate photopolymer with net diffraction efficiency near 100%. *Applied Optics*, 43:2125–2129.
- Suzuki, N. and Tomita, Y. (2007). Holographic scattering in SiO₂ nanoparticles-dispersed photopolymer films. *Applied Optics*, 46:6809–6814.
- Suzuki, N., Tomita, Y., and Kojima, T. (2002). Holographic recording in TiO₂ nanoparticle-dispersed methacrylate photopolymer films. *Applied Physics Letters*, 81:4142–4123.
- Suzuki, N., Tomita, Y., Ohmori, K., Hidaka, M., and Chikama, K. (2006). Highly transparent ZrO₂ nanoparticle-dispersed acrylate photopolymers for volume holographic recording. *Optics Express*, 14:12712–12719.
- Takayama, S., Nagaya, K., Momose, K., and Tomita, Y. (2014). Effects of symbol modulation coding on readout fidelity of shift-multiplexed holographic digital data page storage in a photopolymerizable nanoparticle-(thiol-ene)polymer composite film. *Applied Optics*, 53:B53–B59.
- Tanaka, K., Hara, M., Tokuyama, K., Hirooka, K., Ishioka, K., Fukumoto, A., and Watanabe, K. (2007). Improved performance in coaxial holographic data recording. *Optics Express*, 15:16196–16209.
- Tomita, Y., Chikama, K., Nohara, Y., Suzuki, N., Furushima, K., and Endoh, Y. (2006a). Two-dimensional imaging of atomic distribution morphology created by holographically induced mass transfer of monomer molecules and nanoparticles in a silica-nanoparticle-dispersed photopolymer film. *Optics Letters*, 31:1402–1404.
- Tomita, Y., Furushima, K., Ochi, K., Ishizu, K., Tanaka, A., Ozawa, M., Hidaka, M., and Chikama, K. (2006b). Organic nanoparticle (hyperbranched polymer)-dispersed photopolymers for volume holographic storage. *Applied Physics Letters*, 88:071103–1–071103–3.
- Tomita, Y., Hata, E., Momose, K., Takayama, S., Liu, X., Chikama, K., Klepp, J., Pruner, C., and Fally,

- M. (2016a). Photopolymerizable nanocomposite photonic materials and their holographic applications in light and neutron optics. *Journal of Modern Optics*, 63:S1–S31.
- Tomita, Y., Nakamura, T., and Tago, A. (2008). Improved thermal stability of volume holograms recorded in nanoparticle-polymer composite films. *Optics Letters*, 33:1750–1752.
- Tomita, Y., Suzuki, N., and Chikama, K. (2005). Holographic manipulation of nanoparticle-distribution morphology in nanoparticle-dispersed photopolymers. *Optics Letters*, 30:839–841.
- Tomita, Y., Urano, H., Fukamizu, T., Kametani, Y., Nishimura, N., and Odoi, K. (2016b). Nanoparticle-polymer composite volume holographic gratings dispersed with ultrahigh-refractive-index hyperbranched polymer as organic nanoparticles. *Optics Letters*, 41:1281–12884.
- Willis, B. T. M. and Carlile, C. J. (2013). *Experimental Neutron Scattering*. Oxford University Press, Oxford.
- Yeh, P. (1993). *Introduction to Photorefractive Nonlinear Optics*. Wiley, New York.

